Ion cyclotron and heavy ion effects on reconnection in a global magnetotail

R. M. Winglee

Department of Earth and Space Sciences, University of Washington, Seattle, Washington, USA

Received 12 January 2004; revised 21 May 2004; accepted 8 July 2004; published 22 September 2004.

[1] Finite ion cyclotron effects play a significant role in determining the dynamics of the neutral sheet. The demagnetization of the ions facilitates reconnection and produces an electric field perpendicular to the direction of the tail currents. This in-plane electric field drives field-aligned currents and an out-of-plane (or core) magnetic field in conjunction with the generation of flux ropes. In addition to these electromagnetic effects, it is shown that ion cyclotron effects lead to the preferential convection of plasma from the dawnside to the duskside. This convection is consistent with results from single-particle tracking but differs from ideal MHD treatment where the flow occurs symmetrically around the Earth. A physical manifestation of these asymmetric particle trajectories is the wrapping of the field-aligned current between the region 1 currents and the region 2 and/or region 0 currents. In addition, localized density enhancements and depletions are seen in the tail where the local heavy ion density can be substantially elevated over ionospheric conditions. Because of the local density variations, reconnection across the tail is inhomogeneous. Reconnection is initiated postmidnight and then sweeps across to the dawn and dusk flanks within a few minutes. Because of this spatial variation, the ejection plasmoid is actually U-shaped and the subsequent flux rope formation is highly skewed. *INDEX TERMS:* 2744 Magnetospheric Physics: Magnetotail; 2753 Magnetospheric Physics: Numerical modeling; 2788 Magnetospheric Physics: Storms and substorms; 2736 Magnetospheric Physics: Magnetosphere/ionosphere interactions; 2431 Ionosphere: Ionosphere/magnetosphere interactions (2736); *KEYWORDS:* reconnection, multifluid, simulation, magnetosphere, magnetotail, flux ropes

Citation: Winglee, R. M. (2004), Ion cyclotron and heavy ion effects on reconnection in a global magnetotail, *J. Geophys. Res.*, *109*, A09206, doi:10.1029/2004JA010385.

1. Introduction

[2] Magnetic reconnection plays a critical role in determining the morphology of the magnetosphere during substorms and storms. Evidence of reconnection has been growing since the initial observations of negative B_z in the tail associated with substorm onset [e.g., *Hones*, 1976]. While initial models showed a well-defined O-type neutral line within the plasmoid [*Hones*, 1979], subsequent studies have shown that plasmoids can have an appreciable core magnetic field [*Sibeck et al.*, 1984; *Elphic et al.*, 1986; *Slavin et al.*, 1989; *Sibeck*, 1990; *Moldwin and Hughes*, 1991, 1992]. On occasion, the core magnetic field can be as strong as, and in some cases exceed, the lobe magnetic field [*Slavin et al.*, 1995]. The direction of the core magnetic field is usually (34 out of 39 cases) in the direction of the B_y component of the interplanetary magnetic field (IMF) [*Moldwin and Hughes*, 1992].

[3] The core field is also observed to be generally unidirectional, although, on occasion, bipolar B_y signatures are seen in conjunction with bipolar B_z signatures [*Moldwin and Hughes*, 1992]. *Lepping et al.* [1995, 1996] used a force-free model for flux ropes and showed that in both the middle and distant tail regions the average diameter was $\sim 10\ R_e$ and in several instances may be as small as $1-3\ R_e$. The origin of these flux ropes in the magnetotail have been attributed to the currents that are generated when the ions become unmagnetized, while the electrons remain magnetized in the reconnection region. The demagnetization of the ions leads to the violation of the frozen-in theorem conditions and provides the physical mechanism by which reconnection can occur. This resultant magnetic diffusion region is thought to have been observed during a Wind perigee pass [*Øieroset et al.*, 2001].

[4] Theoretical and modeling efforts have increasingly focused on resolving the microstructure of the reconnection region and thereby quantifying the controlling influences of the system. *Drake et al.* [1994] have shown for idealized geometries that reconnection does not occur in the smooth MHD manner but rather occurs through filamentation and kinking of the current sheet. *Winglee and Steinolfson* [1993], *Steinolfson and Winglee* [1993], *Biskamp et al.* [1995], *Ma and Bhattacharjee* [1996], *Zhu and Winglee* [1996], *Pritchett et al.* [1996], *Shay et al.* [1998], and *Birn et al.* [2001] have demonstrated, using a variety of different

0148-0227/04/2004JA010385

codes (including full particle, hybrid, and multifluid), that the Hall term in the generalized Ohm's law plays an important role in controlling the reconnection rate in collisionless plasmas. The importance of the Hall term is that it describes the electromagnetic response to the system as the ions become demagnetized owing to their large ion gyroradius relative to that of the electrons, which remain magnetized. As this demagnetization occurs, the above models all show a highly structured reconnection region with a strong out-of-plane (or core) magnetic field. While the different models can show a variety of different instabilities (including firehose, ballooning, lower hybrid drift, and kink-tearing), they share the common feature of a highly structured magnetic field mapping that goes well beyond that seen in ideal MHD models.

[5] While the above particle and hybrid models are very informative in determining the local structure of the reconnection, the one real problem that has received very little attention is how to place this physics into global models so that direct comparisons with in situ observations of magnetospheric activity can be made. Initial global simulations [*Winglee et al.*, 1998] incorporating the Hall and ∇P in the Ohm's law have shown similar core magnetic field and flux ropes structures, as seen in the above particle and hybrid codes but on the observed scale size of a few R_e. This initial work assumed the presence of only a single ions species within the magnetosphere.

[6] However, the assumption of a single ion species for the magnetosphere is probably not accurate, since during disturbed times the ionosphere can be an important source of plasma to the magnetotail [*Chappell et al.*, 1987] and this outflow can be dominated by heavy ionospheric ions such as O^+ [e.g., *Yau and André*, 1997]. To address this issue, *Winglee* [2000] developed a global model that included the presence of heavy ions. This model as able to provide three-dimensional (3-D) rendering of the geopause (i.e., the boundary within the magnetosphere where the plasma changes from one being dominated by plasma of solar wind origin to one being dominated by plasma of ionospheric origin). More recently, these ionospheric outflows have been shown to produce saturation of the cross-polar cap potential [*Winglee et al.*, 2002].

[7] In this paper we demonstrate that ion cyclotron effects are not only important with respect to the electrodynamics of the system due to corrections in the generalized Ohm's law, but they also have an important effect on the momentum equations for the different ions species. These effects are shown to play a critical role in determining the particle acceleration and convection in the reconnection region and in the structure of the field-aligned currents into the auroral region. Such plasma flows are then shown to modify the reconnection rate across the magnetotail, which in turn modifies the overall structure of flux ropes generated in association with substorm onset.

[8] This work is motivated by the fact that recent single-particle tracking results within the electric and magnetic field from global simulations show dawn-dusk acceleration of plasma [*Winglee*, 2003] consistent with *Speiser* [1965] particle motion. However, this asymmetric particle acceleration does not appear within the ideal MHD. Instead, for southward interplanetary magnetic field (IMF) the flow of plasma from the reconnection region is predicted to occur symmetrically around the Earth. If we are to better model the dynamics of the magnetosphere, then this discrepancy between particle and fluid perspectives needs to be resolved.

[9] In section 2 the formalism behind a fully self-consistent multifluid treatment with ion cyclotron terms included in the electrodynamics as well as the plasma dynamics is described. Note that it is these latter ion cyclotron terms that produce differential convections between the different ion species. While the global code does not have the capacity to resolve all the structures seen in high-resolution hybrid codes, it is demonstrated that Hall and ion cyclotron effects that are incorporated in the global simulations are already sufficient to alter the dynamics of the global magnetosphere.

[10] The presence of heavy ions such as O^+ also adds a new inherent scale length to the reconnection region. This scale length is fully resolved within the global code. In section 3 we demonstrated that while the overall magnitude of the cross-polar cap potential and field-aligned currents remain of the order of that seen in previous simulations, the full inclusion of the ion cyclotron terms modifies the structure of the auroral current system to produce the spiral flow of current between the region 1 and region 2 currents as noted by *Iijima and Potemra* [1976, 1978] using data from the Triad satellite. In other words these apparently small corrections have global consequences for magnetospheric activity. In section 4 we then show the actual structures generated in the tail including the dawn-dusk acceleration of plasma and asymmetric reconnection rate across the tail, with a corresponding distortion of the plasmoid/flux rope topology. A summary of results is given in section 5.

2. Simulation Model

[11] In this section we detail the equations used in the multifluid modeling, including for the first time ion cyclotron corrections to the momentum equations of the different ions species present. A discussion is presented on the relative size of these corrections and why they can at least partially be incorporated into a global model. We also compare and contrast the code capabilities relative to hybrid codes to give more insight into the assumptions being made within the code. The code details are then described.

2.1. Electrodynamics

[12] The dynamics of any fluid plasma component are given by

$$\frac{\partial \rho_\alpha}{\partial t} + \nabla \cdot (\rho_\alpha \boldsymbol{V}_\alpha) = 0 \tag{1}$$

$$\rho_\alpha \frac{d\boldsymbol{V}_\alpha}{dt} = q_\alpha n_\alpha (\boldsymbol{E} + \boldsymbol{V}_\alpha \times \boldsymbol{B}(\boldsymbol{r})) - \nabla P_\alpha - \left(\frac{GM_J}{R^2}\right)\rho_\alpha \vec{\boldsymbol{r}} \tag{2}$$

$$\frac{\partial P_\alpha}{\partial t} = -\gamma \nabla \cdot (P_\alpha \boldsymbol{V}_\alpha) + (\gamma - 1)\boldsymbol{V}_\alpha \cdot \nabla P_\alpha, \tag{3}$$

where ρ_α, P_α, and V_α are the mass density, pressure, and velocity of the component α. MHD is based on combining the above equations to give a single-fluid treatment. The multifluid treatment is based on the same equations, but the

dynamics of the electrons and the different ion species are kept separate. For electrons it is assumed that they have sufficiently high mobility along the field lines that they are approximately in steady-state drift motion. In other words their motion can be described by drift motion (i.e., $m_e\ dV_{de}/dt = 0$) so that

$$\boldsymbol{E} + \boldsymbol{V}_{de} \times \boldsymbol{B} + \frac{1}{en_e}\nabla P_e = 0. \quad (4)$$

Equation (4) is not actually solved for $\boldsymbol{V}_{de}$ but instead is used as an Ohm's law to give $\boldsymbol{E}$, where $\boldsymbol{V}_{de}$ is determined from the induced currents and the assumption of quasi-neutrality, i.e.,

$$n_e = \sum_i n_i, \quad \boldsymbol{V}_{de} = \sum_i \frac{n_i}{n_e}\boldsymbol{V}_i - \frac{\boldsymbol{J}}{en_e}, \quad \boldsymbol{J} = \frac{1}{\mu_0}\nabla \times \boldsymbol{B}. \quad (5)$$

Thus substitution of equation (5) into equation (4) yields the modified Ohm's law of

$$\boldsymbol{E} = -\sum_i \frac{n_i}{n_e}\boldsymbol{V}_i \times \boldsymbol{B} + \frac{\boldsymbol{J} \times \boldsymbol{B}}{en_e} - \frac{1}{en_e}\nabla P_e + \eta(x)\boldsymbol{J}. \quad (6)$$

The first term in equation (6) is the ideal Ohm's law and the last term $\eta(\boldsymbol{x})\boldsymbol{J}$ is added to allow for finite conductivity in the ionosphere. Collisions beyond this region are assumed to be negligible. No anomalous resistivity is included in the code, as the nonideal terms included in equation (6) are sufficient to drive reconnection.

[13] The other terms in equation (6) include the Hall and ∇P terms and are ion cyclotron corrections to the Ohm's law. Such corrections to the Ohm's law are known to be important in terrestrial reconnection studies and can drive field-aligned currents into the auroral region [*Zhu and Winglee*, 1997; *Winglee et al.*, 1998; *Shay et al.*, 1998]. These terms in dimensionless parameters are of order of the ion skin depth (c/ω_{pi}, where ω_{pi} is the ion plasma frequency) relative to the grid spacing Δ_x. In the following, Δ_x is 0.25 R_e (1600 km) in the vicinity of both the dayside and nightside reconnection regions. The ion skin depth for protons assuming a density of 1 cm^{-3} is ~200 km. So for the global model we can set $\Delta_x/(c/\omega_{pi})$ to ~8, whereas in hybrid models this ratio is more typically set to unity. If the plasma sheet density should decline, say during the growth phase of a substorm, then $\Delta_x/(c/\omega_{pi})$ can decrease to ~2–4, so it is not appropriate to assume that this term is always negligible as assumed in ideal MHD.

[14] One might argue that at a value of 8 the global code cannot resolve any ion cyclotron effects in the electrodynamics. For protons, even at a value of 8, gradient B effects are nonnegligible. For oxygen ions, their gyroradius becomes resolvable when they enter the tail and magnetopause current sheets, particularly if they are accelerated to perpendicular velocities above ~100 km/s.

[15] Finite gyroradius effects are not the whole story, as one also needs to take into account collective effects. Consider the actual size of the $\boldsymbol{V} \times \boldsymbol{B}$ terms relative to the $\boldsymbol{J} \times \boldsymbol{B}/en$ term. While fast flows are seen in the in-plane direction, the speeds of plasma flowing in the direction of the current sheet are of the order of 50–100 km/s. Now suppose that the magnetotail is driven into lobe reconnection (i.e., that field lines that were initially in the lobe have sufficient time to convect into the plasma sheet and be reconnected). The lobe field is of the order of 20 nT, and n_e is of the order ~1 cm^{-3} or less. Suppose that the global code can at best resolve the current sheet at a minimum of 3 grid units so that the inherent length scale is 3 Δ_x and $(\boldsymbol{J} \times \boldsymbol{B}/en)/(\boldsymbol{V} \times \boldsymbol{B})$ is of order 20–40%, that is, the strength of the correction term is significant and cannot be neglected.

[16] A similar calculation would show that these corrections are important at the magnetopause but are essentially negligible in the inner magnetosphere where the densities are much higher. Since these reconnection regions determine the particle entry into the magnetosphere and play a critical part in the energization of plasma within the magnetosphere, it is an important starting point to incorporate these nonideal MHD effects into a global code. Presently, there is no other means to incorporate these effects on reconnection on global scale lengths.

2.2. Plasma Dynamics

[17] The description of the electron dynamics is completed by the pressure equation

$$\frac{\partial P_e}{\partial t} = -\gamma\nabla \cdot (P_e\boldsymbol{V}_{de}) + (\gamma - 1)\boldsymbol{V}_{de} \cdot \nabla P_e \quad (7)$$

and the evolution of the magnetic field by the induction equation

$$\frac{\partial \boldsymbol{B}}{\partial t} + \nabla \times \boldsymbol{E} = 0. \quad (8)$$

The ion dynamics is determined by simultaneously time stepping all the individual ion species equations (i.e., equations (1)–(3)) using the electric field in equation (6). These equations are essentially the same as used in hybrid codes except that they are in the fluid limit as opposed to having particle ions. In section 2.3 we will discuss why these numerics can lead to stable solutions despite the fact that ion skin depth is only a fraction of the grid spacing. Before discussing the numerics, though, it is important to look at an explicit substitution of the ion momentum equation using equation (6), which has the form

$$\rho_\alpha \frac{d\boldsymbol{V}_\alpha}{dt} = \frac{q_\alpha n_\alpha}{en_e}(\boldsymbol{J} \times \boldsymbol{B} - \nabla P_e) - \nabla P_\alpha + q_\alpha n_\alpha\left(\boldsymbol{V}_\alpha - \sum_i \frac{n_i}{n_e}\boldsymbol{V}_i\right) \times \boldsymbol{B} + q_\alpha n_\alpha \eta \boldsymbol{J} - \left(\frac{GM_J}{R^2}\right)\rho_\alpha \vec{\boldsymbol{r}}. \quad (9)$$

Equation (9) is essentially the same that has been used in previous multifluid treatments [e.g., *Winglee*, 2003; *Winglee et al.*, 2002] except that the velocity difference term ($\boldsymbol{V}_\alpha - \sum (n_i/n_e)\boldsymbol{V}_i$) is now retained. In MHD all the ion species are assumed to have the same drift velocity and hence the neglecting of this term. This assumption makes a convenient starting point to evaluate point differences in the global dynamics owing to the presence of heavy ions, including the saturation of the cross-polar cap potential.

[18] However, neglecting the above term does not provide a complete description of the system. In fact the fluid flows

that develop with the dropping of this term produces the symmetric plasma flows around the inner magnetosphere for southward IMF. This is contrary to the particle-tracking results that show dawn-dusk acceleration of ions across the tail current sheet. This difference between the actual fluid velocity and a center of mass velocity is very similar to that in particle treatments. In the latter, one splits the particle motion in terms of a drift motion and cyclotron rotation. The small difference in speed that arises from the particle gyrating in an inhomogeneous magnetic field drives the ∇B drift, and this occurs even if the gyroradius is very much smaller than the scale length of the gradient in the magnetic field. The same is true in the present case in that if there are gradients in the magnetic field, then the velocity difference term is nonzero and thereby drives the breaking of the symmetric flows of ideal MHD.

[19] In the presence of different ion species the velocity difference term is in general nonzero owing to finite ion cyclotron corrections. For example, consider a typical current sheet configuration with a magnetic field of 5 nT near the center of the current sheet. For a keV proton the gyroradius is $\sim$600 km. For an O^+ ion at the same energy the gyroradius is 2400 km, which starts to become resolved in the global simulations and can therefore start to experience electric field acceleration. A subtle but important point is that even if the grid resolution is not sufficient to resolve a gyroradius, a particle or fluid element undergoing a gyration within a grid unit will still experience the gradient in the magnetic field (since all properties rely on interpolation between grid points) so that even without full resolution ∇B effects/drifts will still develop if the bulk temperature becomes sufficiently high to become comparable to the convective drifts.

[20] It is also important to remember that the O^+ ions will not remain at the same energy as the protons but in fact will experience preferential acceleration and therefore have an even larger energy and gyroradius. Indeed the particle trajectory analysis of *Speiser* [1965] shows that ions that are ejected from the reconnection region will have speeds of the order of the Alfvén speed irrespective of mass so that the heavy ions will always tend to be preferentially accelerated over light ions. It is for the same reason that protons will be preferentially accelerated over electrons in reconnection regions.

[21] One could suppose that maybe the heavy ions have only a low concentration and possibly have little effect. However, the results of *Seki et al.* [1998, 2001] have shown that O^+ flows can be typically a few percent in the tail. At just 6% number density, the O^+ ions will provide equivalent mass as the protons, and if they attain comparable velocities, as mentioned above, they will also be responsible for equal amounts of energy transport out of the current sheet. Thus the plasma dynamics generated by this seemingly small term can have an appreciable effect on the overall global properties of the magnetosphere. This will also be demonstrated by the simulation results in the following sections.

[22] One of the consequences of retaining this term is that it generates ion cyclotron waves in the system. These ion cyclotron waves appear at both the proton and heavy ion cyclotron frequencies. The heavy ion frequency is not a problem, but the proton cyclotron frequency does add an additional constraint. In particular it requires the simulation time step to be reduced to resolve such waves. With 0.25 R_e resolution and 2.5 R_e inner radius, this requirement produces about a 25–50% reduction in time step, which is not too much of a hardship on the code.

[23] One of the outstanding issues in reconnection is how to produce the demagnetization of the electrons. This is produced in the present code by the generation of field-aligned currents, which are incorporated by the inclusion of the gradient pressure term in the Ohm's law. As reconnection occurs, the field-aligned currents remove electrons from the reconnection region and the return current places away from the reconnection region to match the accelerated ion flows. Effects from the direct acceleration of electrons within the reconnection region are not included in the present model, as we are unable to resolve electron cyclotron effects. It is not known at this time whether the relocation of the electrons from field-aligned currents or their direct acceleration in the reconnection region is the dominant process in pulling electrons off the reconnection field lines. However, the development of field-aligned currents as described here has been seen in full particle simulations, albeit in more restricted geometries [*Winglee and Steinolfson*, 1993; *Zhu and Winglee*, 1996].

2.3. Numerical Algorithm and Boundary Conditions

[24] The above equations are solved for a three-ion component plasma: solar wind protons, ionospheric protons, and ionospheric O^+ ions. On including the electron dynamics, the code provides a four-fluid description of the global magnetosphere. The equations for each of these components is solved using a two-step Lax-Wendroff differencing scheme [*Richtmyer and Morton*, 1967] with Lapidus smoothing on plasma properties only [*Sod*, 1978]. The latter is required to remove unphysical grid point oscillations across sharp discontinuities such as the bow shock. While the two-step Lax-Wendroff scheme is one of the simpler numerical methods, its simplicity allows a tractable means for including much more complicated but more realistic physics. Another reason for using this scheme is that we can track how the evolution of the system changes as additional ion cyclotron terms are added relative to previously published treatments [*Winglee et al.*, 1998, 2002; *Winglee*, 2000]. As shown in the following section, because the scheme is well validated the development of dawn-dusk asymmetries in the magnetosphere is due to physical processes associated with the inclusion of ion cyclotron and heavy ion mass loading effects and is not due to numerics.

[25] At this point there is a major divergence between the multifluid codes and the hybrid codes. Hybrid codes accumulate the ion density on the grid to be used in the Ohm's law given by equation (6). As such they have the advantage of being able to incorporate effects from non-Maxwellian distributions, which the fluid code cannot. Hybrid codes have the disadvantage, though, in that they are subject to grid point noise due to particle statistics. Such grid point noise, particularly in the electric field, can eventually lead to numerical instabilities. The use of Lapidus smoothing in the fluid code eliminates the growth of such grid point instabilities. It is for this reason that the multifluid code can operate in a regime where the ion skin depth is only a

fraction of a grid spacing. The downside, of course, is that we lose all the physics associated with very small scale processes seen in higher-resolution hybrid code, but we have the advantage that a full global magnetospheric model can be developed with ion cyclotron effects incorporated in key regions. Here we show that even with this limited treatment such ion cyclotron terms can produce substantial effects. The equations are solved on a structured Cartesian grid using a box-in-box grid system.

[26] The grid system allows for high 0.25 R_e resolution over much of the inner plasma sheet, while allowing the incorporation of a total system size of 200 R_e down tail and ± 50 R_e in the y, z directions at $1-2$ R_e resolution. The solar wind boundary is at $x = 35$ R_e. The inner boundary is set at 2.5 R_e. To simulate the Earth's resistivity, the region within the inner boundary is given a finite resistance equivalent to a Reynolds number of 10. At the actual inner boundary (representing the ionosphere), the Reynolds number is increased to 20 and at one grid point above it is set at 40. At all other points the resistivity is zero. Zero dipole tilt is assumed in the following.

[27] The choice of placing the resistivity at the inner boundary provides only a crude model for the ionosphere. We have performed sensitivity tests of the results, and to date key indicators such as the cross-polar cap potential have been shown to be insensitive to the choice of the ionospheric resistivity. The reason for this insensitivity is that the ionospheric response is not just due to its conductivity but also through the ionospheric outflow rate. The reason for this insensitivity can be thought as follows. The amount of solar wind momentum transferred to the magnetosphere is, to first order, determined by the size of the magnetosphere and its ability to couple to it, which is controlled by prevailing IMF conditions and the solar wind speed and density. This momentum transfer therefore sets the speeds of the convective flows within the magnetosphere. These flows set the convection electric field through some type of Ohm's law such as given in equation (6). Integration of this electric field sets the cross-polar cap potential. Thus changing the conductivity will have little effect on the momentum transfer and therefore little effect on the cross-polar cap potential.

[28] However, if the mass loading of the magnetosphere is altered by induced ionospheric outflows, there will be a corresponding change in cross-polar cap potential which in turn will appear as a change in the overall conductivity of the system (for example if the potential drops without a corresponding drop in field-aligned current). This effect has been demonstrated by *Winglee et al.* [2002]. Thus the key point here is that the ionospheric response is just not conductivity but must also include the known ionospheric outflows mentioned in the introduction. To this end, we place ionospheric protons on the inner boundary with a density of 1000 cm^{-3} and we have a fixed O^+ concentration of 5%. We have retained only a small O^+ concentration in this paper to demonstrate that even for very small concentrations of O^+ the tail dynamics can be substantially modified over that from just a single fluid treatment such as MHD. As discussed in the following section, these boundary conditions produce outflow rates of the order of 10^{25} H^+ ions/s and 10^{24} O^+ ions/s. Because the density and temperature at the inner boundary are held fixed, precipitating energetic plasma is lost from the system. At the outer boundary the flows are supersonic so that open boundary conditions are used, except at the left-hand boundary where the solar wind conditions are specified.

[29] The temperature of the plasma is kept low over the poles but is increased toward the equator to take into account the presence of hotter trapped populations there. To ensure equilibrium along each flux tube, they are initially loaded with a constant value (set by mapping the simulation grid point along the dipole field line to the equator and giving all points along the field line the value prescribed to the equator). The equatorial bulk temperature is set to $\sim$60 eV and in the polar cap it is less than 0.3 eV. The low temperature over the polar cap is typical of conditions there and ensures that much of the ionospheric O^+ is gravitationally bound, and forcing by the solar wind (for example, by centrifugal acceleration [*Cladis*, 1986]) is required to drive heavy ion outflows.

[30] An equilibrium for the magnetosphere is established by blowing in the solar wind from the left-hand boundary for a period of 2.75 hours. The solar wind density is held fixed at 5 cm^{-3} and a speed of 450 km/s with zero IMF. Having established this equilibrium, a southward IMF of -8 nT is imposed for 80 min. This time scale ensures dissipation of transients associated with the southward turning of the IMF and the ejection of a tail plasmoid. A northward turning of the IMF of +8 nT is then imposed to investigate the release of energy stored in the current sheet.

3. Ionospheric Response

[31] In this section we establish the fact that the ion cyclotron effects do not change the overall response of the system in the form of the total auroral currents and cross-polar cap potential, but they do change the structure/spatial distribution of the auroral currents. To see this, Figure 1 shows the timing of the imposed IMF changes relative to the induced changes in the integrated field-aligned currents into the northern hemisphere (positive is for downward currents and negative is for upward currents) and the corresponding cross-polar cap potential. It is seen that the southward IMF can induce currents of the order of a few MA, which is $\sim$10 times greater than the value for northward IMF conditions. The cross-polar potential is driven from $\sim$20 kV to a steady-state value of $\sim$50 kV. These values are comparable to other substorm case studies [*Weimer et al.*, 1992].

[32] An important feature to note in Figure 1 is that the buildup of the auroral currents is slower than the buildup of the cross-polar cap potential. The latter reaches a peak value at 70 kV by T = 0300 and then subsides to its steady-state value, whereas the field-aligned currents have a period of rapid increase up to T = 0308 and then maintain a steady increase up to the time when the northward IMF reaches the magnetosphere.

[33] The data in Figure 1 can be used to attain useful characteristics of the ionospheric response in terms of V/I for an effective ionospheric resistivity (Figure 2a) and V $\times$ I for an estimate of the Ohmic power into the ionosphere (Figure 2b). It is seen from these figures that while the actual ionospheric resistivity is held fixed, the effective resistivity of the ionosphere drops during the southward

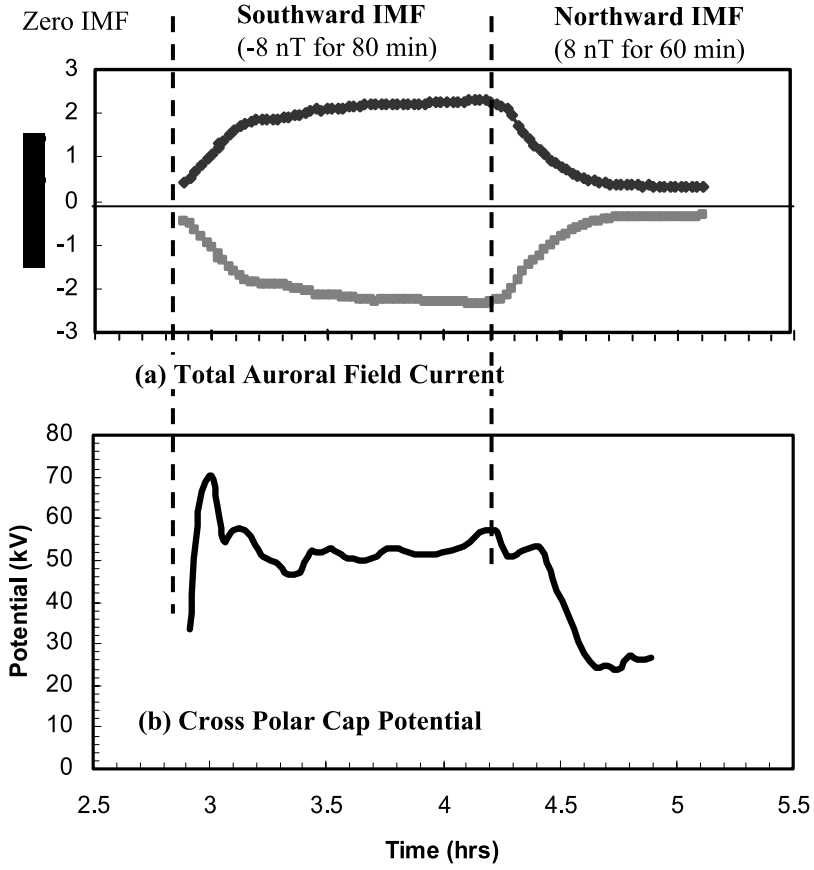

Figure 1. Time history of (a) the integrated field-aligned currents (I_A) into the ionosphere (black for downward currents and gray for upward currents) and (b) the cross polar cap potential (V_P). A 2.75 hour period of zero IMF is used to produce an initial equilibrium magnetosphere. The focus is then on the response of the magnetosphere to a subsequent 80 min period of strong southward (−8 nT) IMF followed by 60 min of strong northward IMF. The cross polar cap potential responses much faster than the currents, similar to a highly inductive system.

IMF period by a factor of 4. The magnitude of the ionospheric resistivity and the percentage decrease are consistent with observed characteristics of ionospheric resistivity. The magnitude of the Ohmic power shown in Figure 2b of ∼100 GW is also consistent with typical estimates for power dissipation in a substorm [e.g., *Lu et al.*, 1996]. Note that while the cross-polar cap potential reaches a steady-state value, the continuous rise in the auroral currents during the period of southward IMF leads to increasing power dissipation in the ionosphere until the effects of the northward turning in the IMF appear in the ionosphere.

[34] The response of the cross-polar cap potential can be understood from the induced ionospheric outflows. These outflows are shown in Figure 3 as they pass through a sphere located at 4 R_e. Prior to the arrival of the southward IMF, the O^+ outflow is ∼1/50 of the ionospheric H^+ outflow. This ratio is smaller than the assumed relative concentration at the ionosphere because with little forcing the heavy ion outflow is gravitationally bound. With the arrival of the southward IMF, the ion outflow for both species increases but with the light ion outflow reaching saturation first at T ∼ 0300. The heavy ions with their larger inertia reach their peak value much later at T = 0330. At this point the relative outflow of heavy ions is ∼1/6 to 1/10 of the light ion outflow. This relative increase arises because the heavy ions are being energized to overcome gravity at lower altitudes to create outflows substantially larger than would have occurred from their thermal outflow alone.

[35] It is important to note that the magnitude of the light ion outflow is consistent with the results of *Yau and André* [1997], but if anything we are underestimating the heavy ionospheric outflow by at least a factor of 2. This underestimation arises because the ionospheric O^+ relative density is held fixed at 5%. Enhancing ionospheric outflows would produce further modification of the cross-polar cap potential [*Winglee et al.*, 2002]. The important point is that as far as the overall ionospheric response is concerned, the boundary conditions assumed in the code (as described in section 2.3) are not extreme and appear to quantitatively reproduce typical ionospheric bulk properties.

[36] The difference in the time response of the heavy and light ionospheric ions is further illustrated in Figure 3b, which replots the outflows in terms of the ionospheric currents calculated from the simulations. It is seen that both the light and heavy outflows show a hysteresis-like curve, but the response time is different for the light and heavy ions. For the light ions the curve associated with increasing current (southward IMF) essentially overlaps the curve for

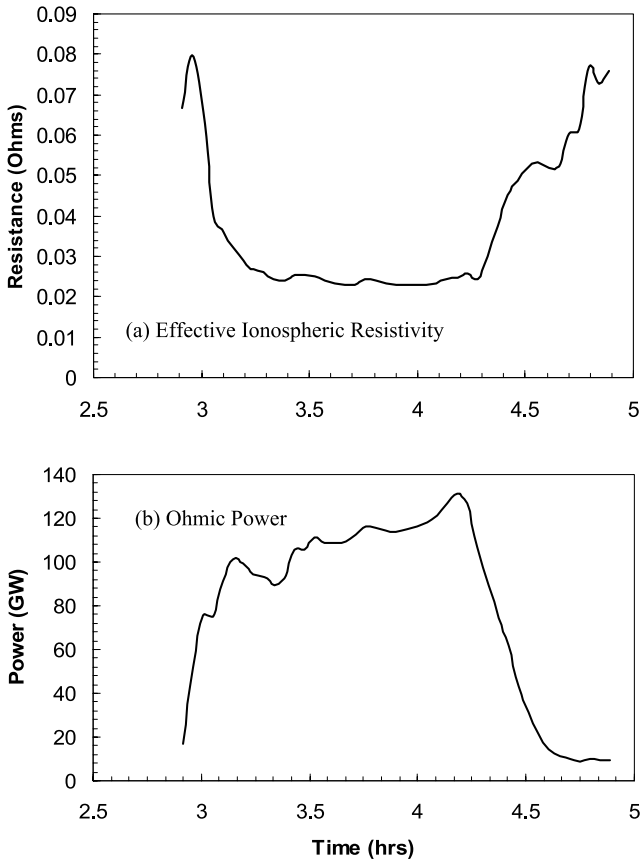

Figure 2. (a) The effective plasma resistivity (V_P/I_A) and (b) the effective Ohmic power ($V_P \times I_A$) using the data in Figure 1. The effective plasma resistivity drops by nearly a quarter during the period of southward IMF, whereas the Ohmic power shows an initial steep rise to ~80–100 GW associated with the rapid raise in the cross polar cap potential, followed by a slower increase to a peak power of 130 GW as the auroral currents slowly increase under continued southward IMF.

decreasing current (northward IMF). For the heavy ions the rate of increase with auroral current is steeper than for the light ions and hangs longer at high values during the initially northward turning of the IMF but eventually returns to its initial quiet time value. The reason for this longer hang time is that the outflow is measured at 4 R_e, so it takes some time for the heated heavy ionospheric ions to reach the measuring point. At the end of the period considered, the O^+ flux is seen to be dropping very much faster than the H^+ outflow.

[37] The effect of ion cyclotron terms in the actual structure of the aurora current system is shown in Figure 4. For north/south IMF conditions the mapping of the field-aligned currents in ideal MHD should be antisymmetric about the noon-midnight meridian. At T = 0250 this is approximately the case, although for zero IMF there is a slight asymmetry with upward current region extending slightly farther down in latitude that the downward current region. As the IMF turns southward (T = 0313), there is both an increase in the peak value of the current density and an expansion in latitude of the current systems. Beyond this time, the peak value does not change significantly but the area does (e.g., T = 0337 and 0410). This increasing area corresponds to the period of slow increase in the total current seen in Figure 1. Note that as the area is increasing the asymmetry in the current system also increases, with the dawnside downward region 1 current system wrapping around through noon to the dusk region 2 current, while the duskside upward region 1 wraps through midnight onto the dawnside region 2 current system. This nightside wrapping of the current extends into the period of northward IMF for ~20 min but eventually fades as the magnetosphere becomes dipole-like under northward IMF. During the northward IMF the dayside wrapping of the near-noon region 1 current into the region 0 current becomes more pronounced (e.g., T = 0420 and 0430).

[38] The wrapping of the auroral current systems seen in Figure 4 is an important feature. The wrapping of the current systems was first noted by *Iijima and Potemra*

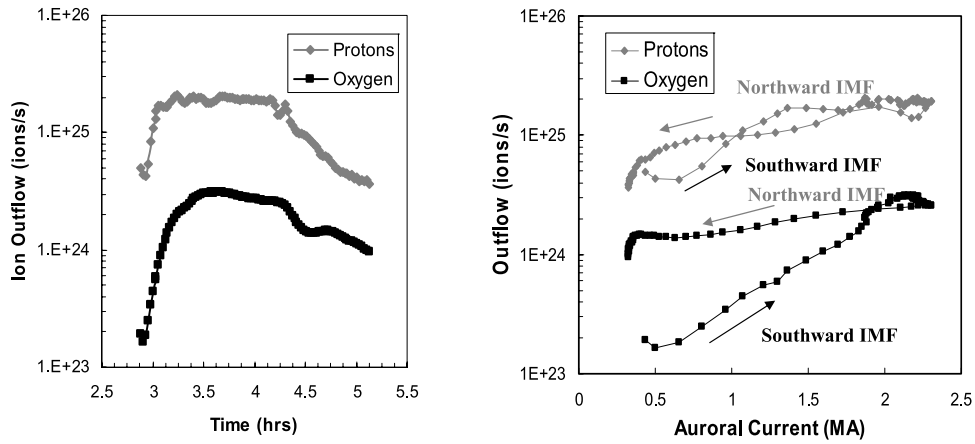

Figure 3. The induced ionospheric outflows (calculated at a radius of 4 R_e) for the assumed ionospheric conditions as a function of (a) time and (b) the auroral currents as shown in Figure 1. The magnitudes of the outflows are comparable to fluxes report by *Yau and Andre* [1997] with the O^+ flux if anything being on the low side. As a function of auroral current, the outflows form hysteresis curves with the heavy ions having a sharper slope and a longer recovery time.

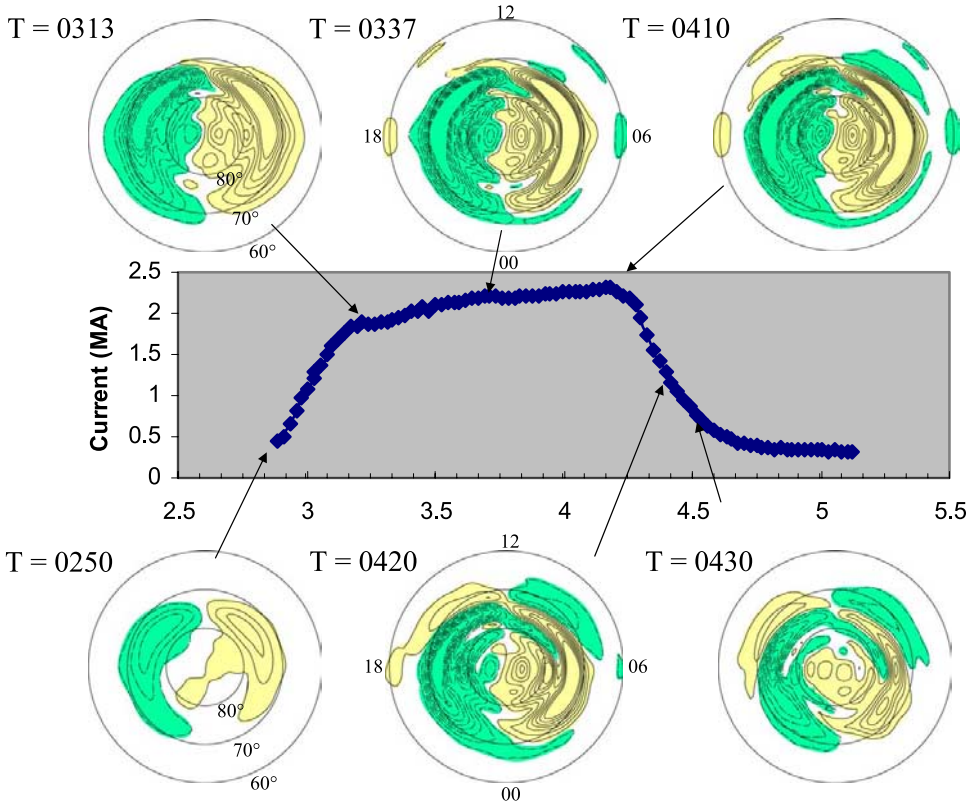

Figure 4. Evolution of the spatial distribution of the auroral currents. Upward current regions are shown in green and the downward currents are shown in yellow. The retention of ion cyclotron terms in momentum equation breaks the symmetry in the auroral current system to produce wrapping of the nightside dusk region 1 current to the dawnside region 2 currents and the dayside dusk region 1 current to the region 0 dawn current and the dayside dawn region 1 current to the dusk region 2 current. The latter two connections are seen to continue after the northward turning of the IMF.

[1976, 1978], using statistical maps of the field-aligned currents. Their results are shown in Figure 5a. One can check the physical origin of this feature evaluating the auroral currents with different ion cyclotron corrections included. Figure 5b shows the results under exactly the same conditions but only the ideal MHD equations are solved. These results, similar to *Ogino et al.* [1986], show an antisymmetric current system and no wrapping of the aurora current across the noon-midnight meridian is present. Figure 5c shows the results using the original version of the multifluid simulations [e.g., *Winglee*, 2000; *Winglee et al.*, 2002]. This version includes the Hall and gradient pressure corrections to the Ohm's law but neglects the finite ion cyclotron terms in the momentum equation (i.e., all the ions were assumed to have the same perpendicular drift speed). The same O^+ concentration of 5% is assumed. It is seen in this case that there is partial breaking of the MHD antisymmetry with partial extension of the dusk region 1 current across the noon-midnight meridian but nothing to the extent reported by *Iijima and Potemra* [1976, 1978].

[39] Figure 5d shows the present results with ion cyclotron corrections in both the Ohm's law and momentum equations. It is seen that the wrapping of the nightside currents is enhanced with the dawnside and duskside region 1 currents crossing the noon-midnight meridian both near noon and near midnight. The present system produces the best agreement to date with the *Iijima and Potemra* [1976, 1978] pattern. The main discrepancy is that our region 2 current is not intense enough to show at local times near midnight. This probably arises because much of the ring current is carried by particles in the tail of the distribution, and the physics of such energetic tails is not well incorporated in fluid treatments.

4. Magnetospheric Response

4.1. Density Variations

[40] In this section we consider the changes in the structure of the magnetosphere associated with the field-aligned currents and ionospheric outflows described in the previous section. The overall behavior of the composition of the magnetosphere is similar to previous multifluid simulations [*Winglee*, 2000] in that with the turning of the IMF to increasingly stronger southward IMF, the solar wind density within the magnetosphere drops. This is illustrated in Figures 6a and 6b where the lobes first become depleted and the current sheet thins (as seen by the cross-plane cuts). However, a key difference is that this thinning does not occur at a uniform rate across the tail, and instead there is a thick high-latitude band of solar wind plasma that penetrates into the lobe across the duskside.

[41] After ~30 min from the southward IMF turning, the contributions of the solar wind plasma to the tail current sheet falls to lobe-like densities at less than 0.01 cm^{-3}

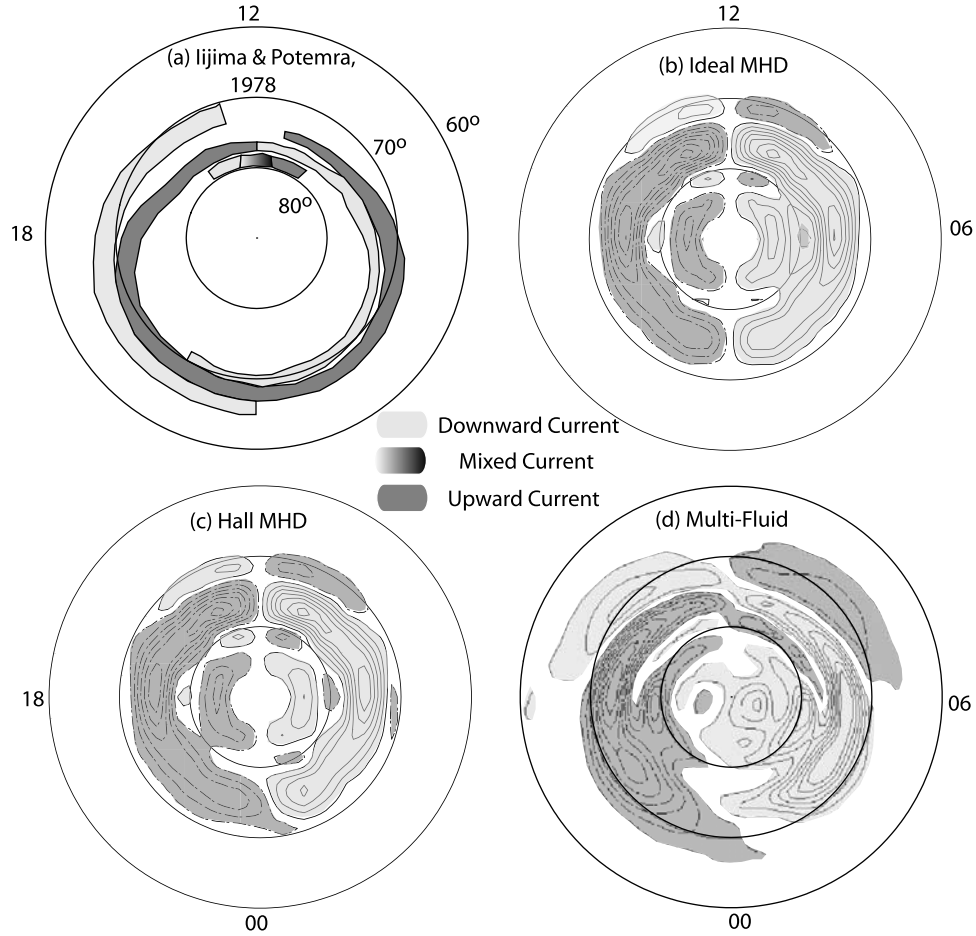

Figure 5. Comparison of the auroral field-aligned current systems from (a) *Iijima and Potemra* [1978], (b) ideal MHD, (c) multifluid treatment with ion cyclotron corrections in the Ohm's law only, and (d) the present multifluid treatment with ion cyclotron treatments in the Ohm's law and momentum equations. As the nonideal effects are added, the simulation results converged on the wrapped field-aligned currents of *Iijima and Potemra* [1978].

(Figures 6c and 6d). The last region of the current sheet to be depleted of solar wind plasma is on the premidnight sector. This lag occurs because the plasma is subject to current sheet acceleration that preferentially transports the plasma from the dawnside to the duskside. With the northward turning of the IMF, solar wind plasma enters through the flanks (by high-latitude reconnections and the subsequent convection of newly closed field lines around the flanks). The midtail region at $30-60\ R_e$ is first to refill (Figure 6f), with the dawnside having greater penetration of solar wind plasma than the duskside.

[42] The dawn-dusk asymmetries are even more apparent in the density of the ionospheric contributions to the magnetosphere, as shown in Figures 7 and 8. At the first time shown in Figure 7, the ionospheric H^+ ions are present through most of the current sheet except for the depletion regions near the inner edge of the plasma sheet. Because of the relatively thick current sheet (since the forcing from the IMF is relatively weak at this time), ionospheric H^+ is seen at high latitudes as well as in the cross-tail cuts in Figure 7a. With strong southward IMF, this high-latitude plasma is convected into the plasma sheet so that while their density in the lobe decreases in Figure 7b, their contributions to the plasma sheet increase (Figure 7c), except near the depletions regions, which actually increase in size. The depletion regions develop because the nightside source is convected into the sheet closer in toward the Earth, while the dayside (cusp/cleft) source convects much deeper into the tail, similar to the particle tracking results of *Winglee* [2003].

[43] As the current sheet continues to thin under the influence of southward IMF, the current sheet tends to be relatively depleted of ionospheric H^+, similar to the solar wind protons. There is a limited range of local times where high-density channels appear, and these channels, as shown below, are associated with reconnection in the tail. These channels lie preferentially on the duskside (Figure 7d) and are seen only if the ion cyclotron term is kept in the momentum equation. Another asymmetry that develops is a dayside bulge associated with the enhanced plasmaspheric plasma convection near noon and is associated with wrapping of the region 1 and 2 currents shown in Figure 4.

[44] The evolution of the heavy ion density shows stronger ion cyclotron effects, but because their gyroradius tends to be much larger than the proton gyroradius these features do not necessarily coincide with those of the ionospheric protons. This is seen for example in Figure 8a where a

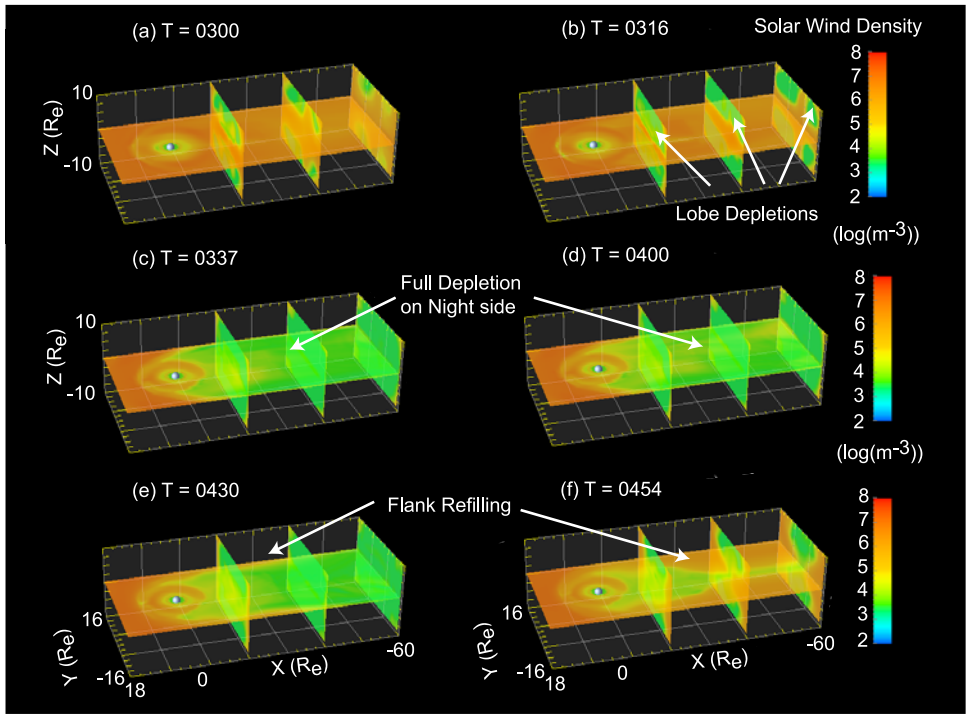

Figure 6. Evolution of the solar wind density as seen by equatorial density contours and three cross-tail cuts at x = 15, 30, and 60 R_e. Southward IMF leads to the depletion of the solar wind component within the magnetosphere with the duskside being the last to become fully depleted. The northward turning of the IMF leads to the reentry of solar wind plasma by high-altitude reconnection and subsequent convection of the newly reconnected field lines into the magnetosphere.

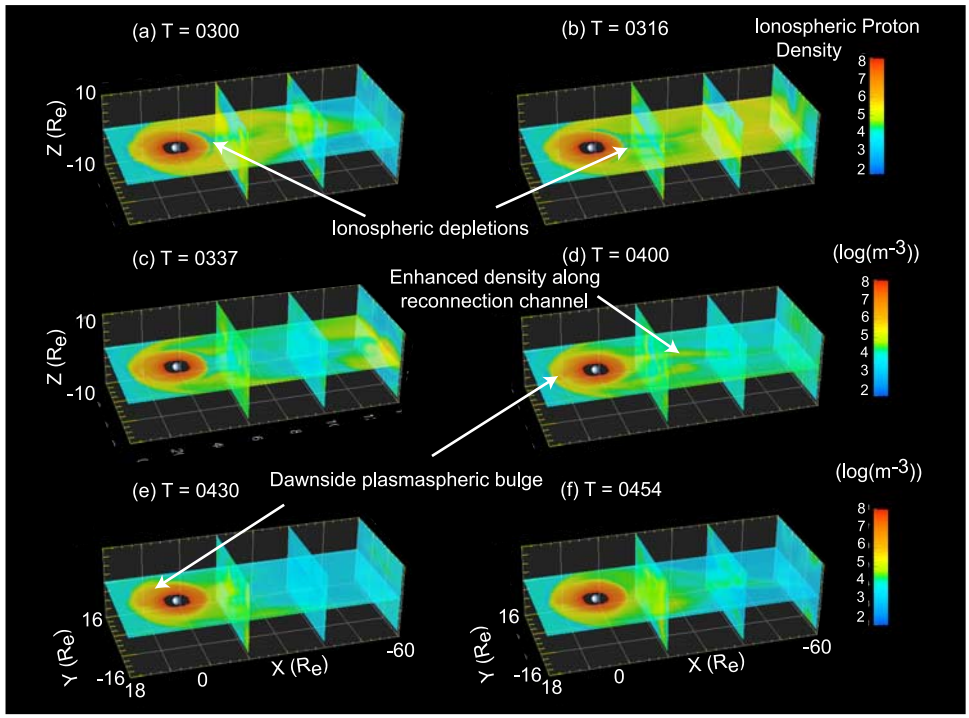

Figure 7. As in Figure 6, except the evolution of the density of ionospheric H^+ is shown. The H^+ density in the magnetosphere also declines during southward IMF, but there are narrow filaments of enhanced density that extend down the tail between midnight and the dusk magnetopause. These filaments are only seen when ion cyclotron effects are included in the ion momentum equation.

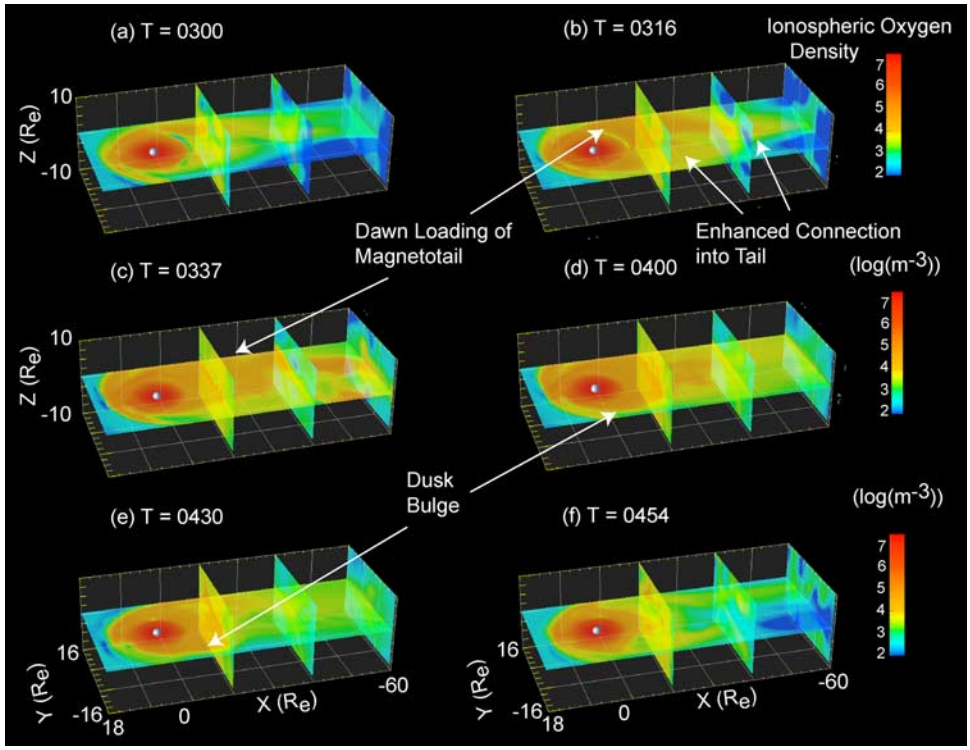

Figure 8. As in Figure 6 except for ionospheric O^+ ions. The dawnside under southward IMF is initially loaded with the heavy ions, similar to single particle trajectories of *Winglee* [2003]. This plasma is convected across to the duskside to produce a bulge in the plasma density near the dusk terminator. An additional bulge near noon is also seen.

dawn-dusk asymmetry at early times during zero IMF is much more evident. The southward IMF enables convection of the heavy ions into the near-Earth plasma sheet, but the thin channels seen in the protons in Figures 6c and 6d are not present in the O^+ in Figures 8c and 8d. The loading of the plasma sheet is seen to spread from postmidnight across to the dusk terminator (Figures 8b–8e). Thus similar to the single particle trajectories of *Winglee* [2003], heavy ion outflows from the dawn to midnight sectors feed the tail current sheet, and this plasma is accelerated across to the dusk sector.

[45] The relative density of O^+ (i.e., $(n_O/\sum n_i)$) is shown in Figure 9 and highlights the differences associated with the different convection patterns of the different ions species. Initially (Figure 9a), the O^+ concentration in the inner magnetosphere is at the 5% level or lower except in the lobe, where the fast speed of the light ions leaves an O^+ rich region at the high latitudes in the lobes. As the IMF turns southward, the greater inertia of the heavy ions causes them to be the dominant species in the plasma sheet boundary layer (PSBL), as seen in Figure 9b. At this stage, despite the fact that the ionospheric O^+ relative concentration is held fixed at 5% at the inner boundary and that their relative outflow rate is relatively low, the O^+ ions in the PSBL can at least temporarily reach relative densities as high as nearly 50%.

[46] When these ions are driven into the tail current sheet, O^+ rich streams are seen in the near-Earth region, as shown in Figure 9c. The stream that forms near midnight is seen to convect around the duskside (Figure 9d), while at the same time the two closest cross-tail cuts in Figure 9d show a lobe that is rich in O^+, particularly on the duskside. With the northward turning of the IMF the O^+ rich regions in the equatorial regions fade, leaving only local regions in the lobe with a high O^+ concentrations.

4.2. Effects on Reconnection

[47] Because of the inhomogeneities in the plasma densities, the reconnection rate across the tail varies between the dawn and dusk flanks. The reason for this is that the convection of plasma into the reconnection region depends on the Alfvén speed, and this is a function of the plasma density, which in turn is dependent on the plasma composition. If plasma is convected from the dawnside to the duskside as seen in the previous subsection, then the reconnection rate will occur relatively faster on the dawnside than on the duskside. To see these differences in the reconnection rate, Figure 10 shows the evolution of B_z in the equatorial region leading up to reconnection in the tail. The figure uses a saturated color table to highlight the separation of regions of positive B_z (red) from negative B_z (blue). The exact position of the neutral line ($B_z = 0$) is shown as the black curve in the plots. For the first time shown, B_z in the magnetosphere is primarily positive while the IMF is negative. The first signs of the formation of a near-Earth neutral line are seen in Figure 10d with the reconnection region appearing postmidnight.

[48] The reconnection region expands rapidly into the dawn and dusk sectors within 3 min. The dusk sector, though, is slower to fully reconnect, as evidenced by the fact that the width of the reconnection regions necks down in Figure 10e and the deepest regions of negative B_z at least

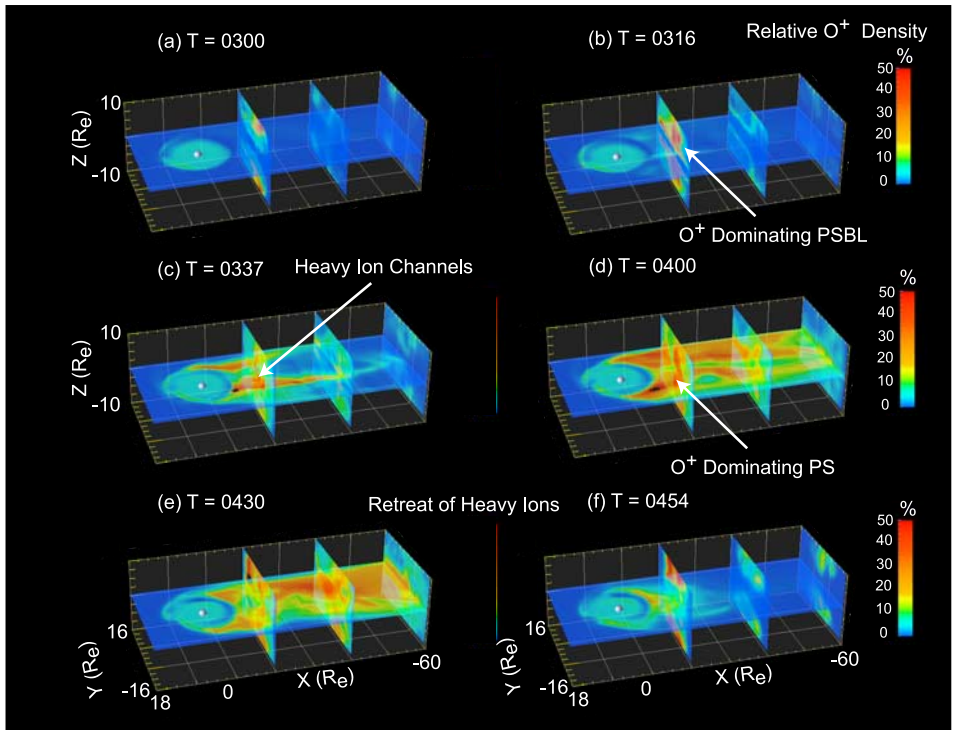

Figure 9. The density of O^+ in the magnetosphere relative to the total ion number density. While the outflow rate of O^+ is always smaller than that for H^+, limitations in access of H^+ to certain regions within the magnetosphere leads to regions that are substantially enhanced in O^+, particularly during periods of strong southward IMF. These locally enhanced regions are also seen in the particle tracking results of *Winglee* [2003].

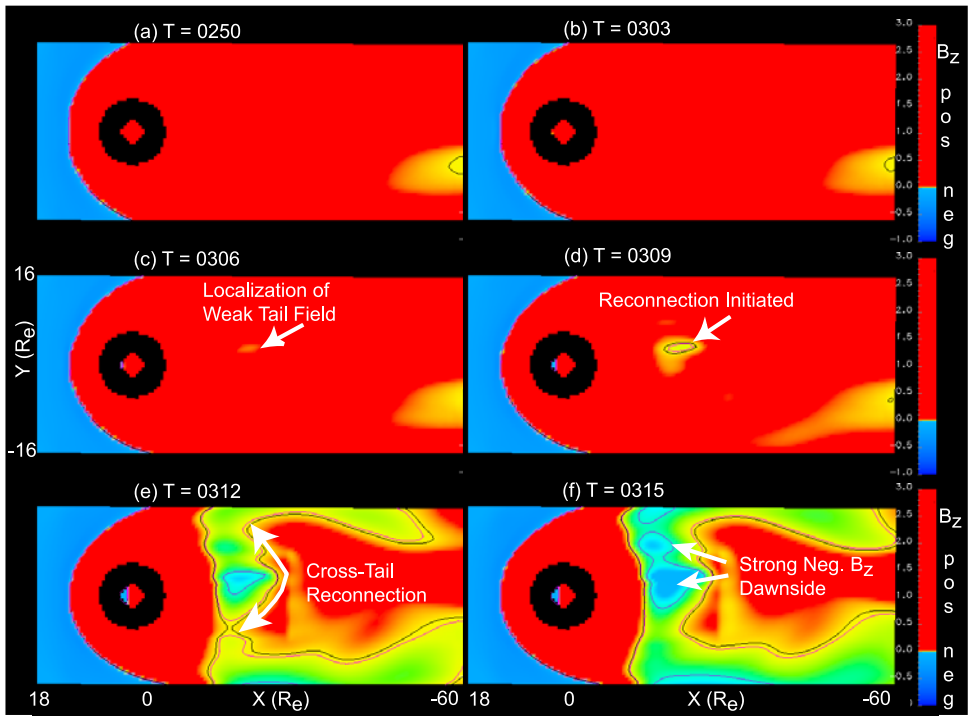

Figure 10. Evolution of B_z in the equatorial plane. A saturated color table is used to highlight the formation of the near-Earth neutral line. The black line shows the contour level for $B_z = 0$. The neutral line is seen to spread rapidly across the tail, with the dawnside initially becoming more negative than the duskside due to the fact that dawn-dusk convection tends to deplete the dawnside of plasma faster, which facilitates an enhanced reconnection rate.

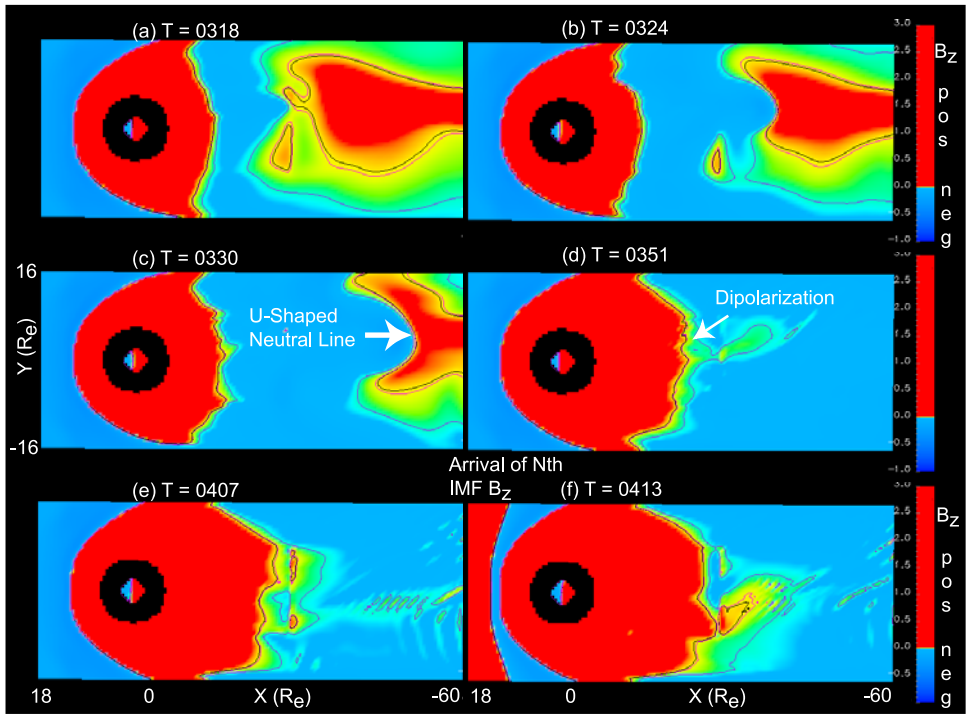

Figure 11. Continuation of Figure 10. Plasmoid ejections occurs via a U-shaped neutral line, and within subsequent depolarization showing the presence of filamentary incursion of positive B_z down the tail, similar to the filaments seen in the plasma density.

at early times are on the dawnside (Figure 10f). Note also that the reconnection does not occur in a homogeneous manner but instead shows filamentary structures that track the density filaments described in the previous subsections. In other words the density structure and composition in the tail is critical to how reconnection actually develops in the region.

[49] The inhomogeneities in the reconnection rate ends up producing macroscopic changes in the ejection of the plasmoid and associated structure in the tail. These global consequences are illustrated in Figure 11, which shows a continuation of the evolution of the reconnection region. It is seen that the development of the reconnection region expands tailward faster along the postmidnight sector, with the dawn sector following and the dusk sector being the most tardy (Figures 11a–11c). This leads to the formation of U-shaped reconnection region, whereas as in ideal MHD simulations the reconnection occurs almost uniformly across the tail.

[50] Partial depolarization occurs while the IMF is still southward, as seen in Figures 11c–11e, with the expansion of the region of positive B_z in the nightside inner magnetosphere from 15 R_e to ~22 R_e. This recovery, like the initial reconnection, is not homogeneous but instead has local regions of positive B_z with the duskside having a longer tailward extension of positive B_z than the dawnside (Figures 11d and 11f).

[51] The effect of the above inhomogeneities on the magnetic field structure is shown in Figure 12, which shows a top view of field lines superposed on contours of the total plasma pressure in the equatorial plane. From this top view, reconnection is not seen until Figure 12c where a small flux rope is first seen to develop in the postmidnight sector. The presence of the flux rope is due to the nonideal MHD terms incorporated in the Ohm's law and has been seen in other simulations [*Zhu and Winglee*, 1996; *Winglee et al.*, 1998]. This ensuing plasmoid grows in size (Figure 12d) but is has a curved front associated with the U-shaped reconnection region seen in Figure 11. Note also that the pressure contours show filamentary structure down the tail into the reconnection region. The filaments arise as plasma is accelerated along the field lines to produce regions low in both pressure and density. These filamentary structures grow in width with the reconnection region.

[52] The flux rope or core magnetic field structure itself is best seen from the side, as shown in Figure 13. The structure basically consists of a flux rope through the center of the plasmoid with the B_y field being comparable to the B_z within ~3 R_e of the core of the plasma (as evidence by the pitch of the flux rope) and is less important further out. The presence of this core magnetic field is consistent with particle simulations of *Zhu and Winglee* [1996] and has similar spatial variation of the core magnetic field reported by *Slavin et al.* [1989] and *Moldwin and Hughes* [1991, 1992]. The plasmoid itself is relatively large with a full down-tail width of 20 R_e.

[53] After the plasmoid ejection, the reconnection activity is dominated by the presence of small-scale flux ropes, as shown in Figure 14. These flux ropes appear ~1 hour after the plasmoid is formed and ejected down the tail. The flux rope has a strong slant from the dawn to dusk sectors. This slant occurs because the dawn sector is depleted in density relative to the dusk sector and as such has a faster reconnection rate than the dayside. The two frames show the

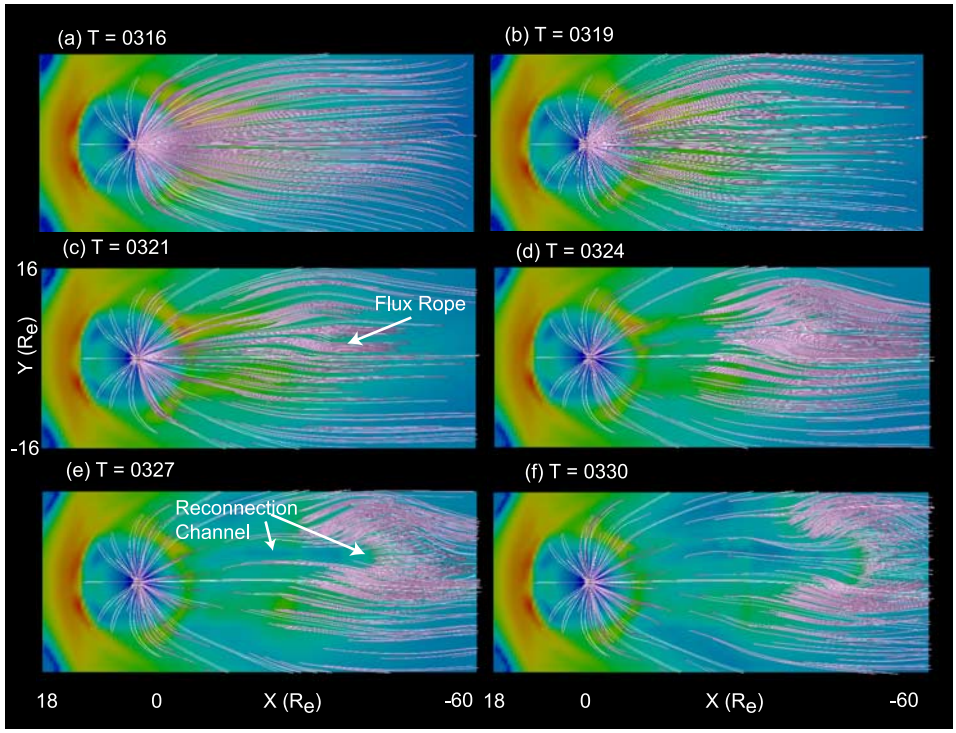

Figure 12. Evolution of the equatorial total plasma pressure and the mapping of the magnetic field in the tail. The U-shaped neutral is clearly manifested in the structure of the plasmoid, and behind it are filamented regions of very low plasma pressure.

faster propagation of the portion of the flux rope on the dawnside relative to duskside. The slanting is also seen in contours of B_z in Figure 11f, where there is a sliver of positive B_z starting at $\sim$30 R_e on the duskside and extending down the tail and crossing over the noon-midnight meridian. These flux ropes have a much smaller scale size than the plasmoid with a lateral width of only a few R_e, which is comparable to the small flux ropes sizes reported by *Lepping et al.* [1996].

5. Discussion

[54] In this paper the possibility of whether small-scale ion cyclotron processes can produce macroscopic effects on the global magnetosphere has been quantitatively evaluated. This is a nontrivial problem because the typical ion gyroradius of a keV proton is of the order of a few hundred kilometers in the vicinity of a neutral sheet and even smaller in the stronger magnetized regions in the inner magnetosphere. On the other hand the magnetosphere itself is tens to a few hundred R_e in size. Because of the disparity in scale sizes ideal MHD is the main tool for global modeling, and in this methodology all ion cyclotron effects are neglected. However, this assumption and the model results lead to an interesting dichotomy. In particular for southward IMF one attains a magnetosphere that has symmetric flows in the inner magnetosphere (neglecting corotation effects), which we know from observations is inaccurate. Single-particle analysis of the current sheet acceleration also shows substantial dawn-dusk asymmetries [*Speiser*, 1965]. The dawn-dusk acceleration is also seen in single-particle trajectories using the electric and magnetic fields of global MHD simulation, despite the fact that the latter has symmetry plasma flows.

[55] In order to try and provide at least a partial resolution of this dichotomy, we have investigated a multifluid treatment of the global magnetosphere incorporating ion cyclotron effects in both the generalized Ohm's law and the ion momentum equation. This present global solution is limited in that it has only a grid resolution in the inner magnetosphere of 0.25 R_e so that the ratio of grid spacing to the ion skin depth is of the order of 2–8 depending on the density in the current sheet. Despite this limitation in grid resolution, the above effects are sufficiently well resolved to produce dawn-dusk asymmetries in the plasma flows and auroral currents.

[56] Key new results are as follows:

[57] 1. Ion cyclotron and heavy ion effects produce a distortion of the auroral currents for purely southward IMF so that there is wrapping of the region 1 currents to the region 2 and 0 current systems across the noon-midnight meridian. This result differs from MHD in that the latter case the currents are required to be antisymmetric across the noon-midnight meridian and as such the field-aligned currents vanish along the noon-midnight meridian. The statistical maps of the field-aligned auroral currents generated by *Iijima and Potemra* [1978] indicate that the physically relevant result should have wrapping of the region 1 currents.

[58] 2. The multifluid code shows dawn-dusk acceleration of plasma in conjunction with the formation of the near-Earth neutral line. As mentioned above, MHD produces

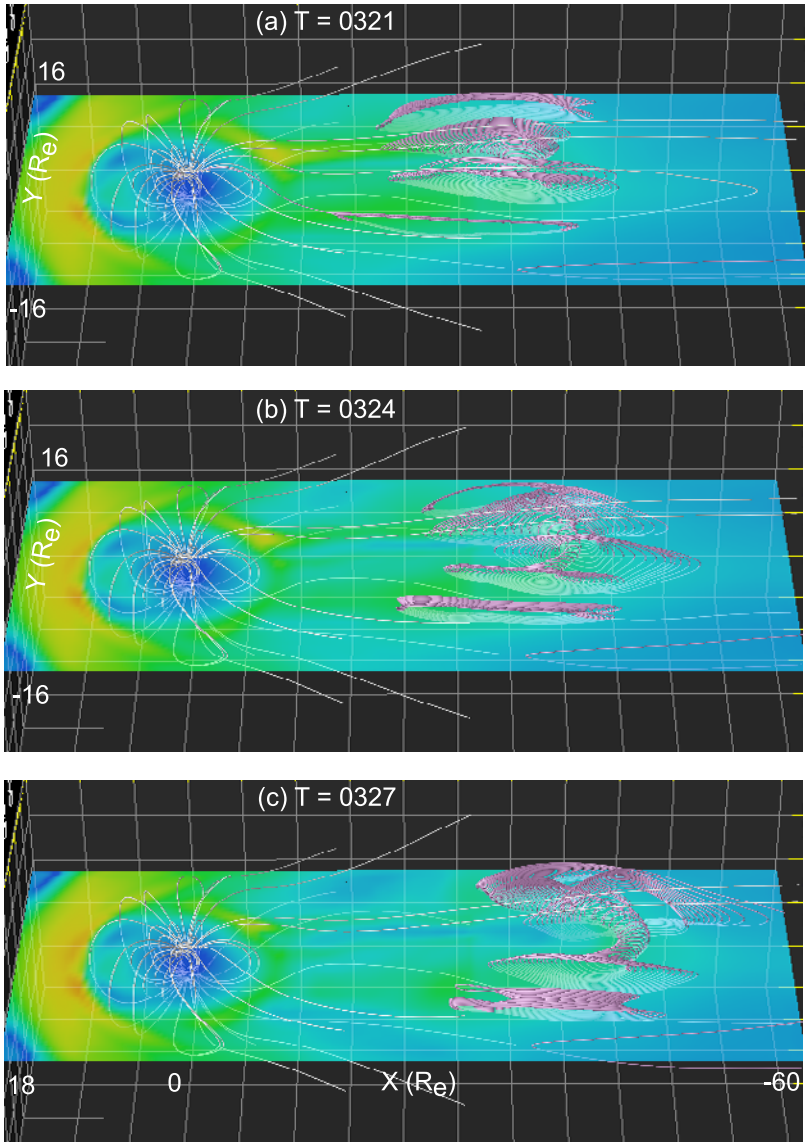

Figure 13. Side view of the magnetic field mapping during plasmoid ejection, superposed on top the equatorial total plasma density. The presence of a strong core magnetic field in the *y*-direction leads to a flux rope structure in the center of the plasmoid, and this flux rope is curved around the U-shaped neutral point.

symmetric flow, whereas as the single-particle analysis shows that dawn-dusk acceleration of ions should be a driving force to the system.

[59] 3. Because of the difference in gyroradius between the heavy and light ionospheric ions, filamentary structures down the tail are predicted, whereas ideal MHD simulations show a structureless reconnection. The presence of bursty bulk flows suggests there is substantial structure occurring in the magnetosphere. Further work needs to establish a link between model results and in situ observations, but the present model makes a very important and testable prediction, specifically that there should be substantial enhancements in heavy ions densities in filamentary structures down the tail associated with reconnection occurring in the tail.

[60] 4. The reconnection does not occur in a uniform rate across the tail due to the dawn-dusk acceleration. This nonuniformity in reconnection rate leads to skewed flux ropes, with the ion cyclotron corrections in the generalized Ohm's law producing a strong core magnetic field. These processes do not occur in ideal MHD. However, the core magnetic field of the present simulations is seen in particle and hybrid simulations of reconnection and is also consistent with the observations cited in the introduction.

[61] Thus the inclusion of finite ion cyclotron and heavy ion effects has global consequences that are consistent with observations and which are omitted in ideal MHD treatments. It is important to note that the code indeed only really resolves ion cyclotron effects near neutral regions. This means that in the strong field regions of the inner magnetosphere, processes such as the formation of the symmetric ring current are not properly described. However, these strong field regions do not typically control the bulk acceleration of ions within the magnetosphere. Instead the region that most influences the bulk particle acceleration

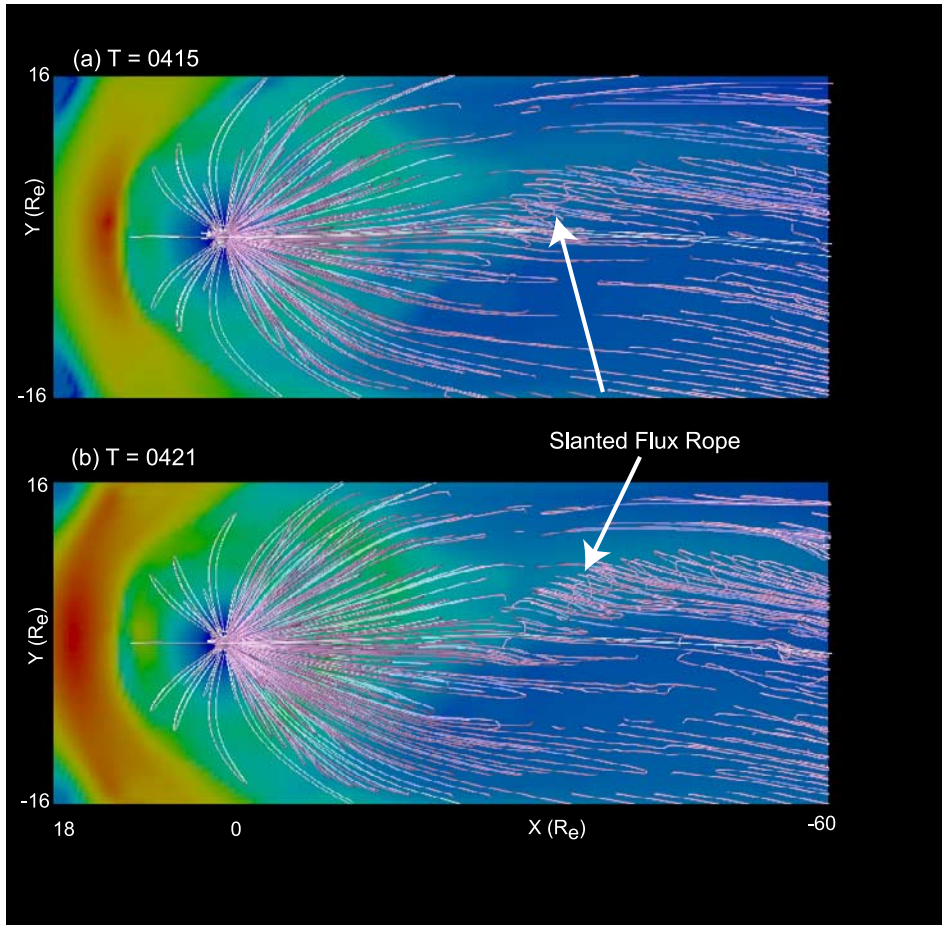

Figure 14. Continuation of Figure 13. A skewed flux rope with narrow width but long extension down the tail is seen after the plasmoid is ejected.

and global flow (transport) is the reconnection region, and the physics of this region is at least partially resolved in the present model.

[62] The question then reduces down to what is the minimum scale length that is relevant to the reconnection region, particularly in the tail, which has been the emphasis in this paper. Clearly the most unstable current sheet in an initial value problem is when the current sheet thickness is of the order of the ion skin depth which is beyond the resolution of the global code. On the other hand the global code is not considering an initial value problem, but instead it treats a driven system controlled by changes in the IMF. As such the system is driven from a thick current sheet to an increasingly thinner current sheet until the point where instabilities prevent further thinning. This inherent scale length is presumably of the order of the ion skin depth.

[63] However, the presence of heavy ions adds a new potentially larger inherent scale length to the system. This large scale length of the heavy ion gyroradius is resolved in the present multifluid simulations. Since these heavy ions will become the first ions to become demagnetized, they will be critical to the formation of the diffusion region around the reconnection region. We have also demonstrated that even for minimal outflow rates, access to the reconnection region is critical to understanding the reconnection problem in the tail.

[64] Under the IMF conditions assumed here as well as in single-particle tracking results of *Winglee* [2003] the light ions have problems accessing the tail reconnection region. Their fast velocity along the field lines tends to make them convect beyond the near-Earth neutral line and therefore have limited access to the reconnection region. On the other hand the model results are consistent with the single-particle studies that show that heavy ions have excellent access and locally can be the dominant ion species. This question of light ion access to the reconnection region further emphasizes the importance of heavy ion mass loading in the magnetotail.

[65] In summary, this paper demonstrates that ion cyclotron terms in both the generalized Ohm's law and the ion momentum equation are important to the dynamics of the magnetosphere, especially in the presence of heavy ionospheric ions. There are two areas where ion cyclotron terms have important consequences. The first is in the electric field where they lead to the generation of the core magnetic field associated with the center of a plasmoid and within flux ropes. The second is in the momentum equations where the corrections lead to a preferential flow of plasma from the dawnside to the duskside as well as produce filamentary structures in the light ions. The physical manifestations of these effects include a reconnection rate that varies across the tail, a skewing of the flux ropes generated in the tail, and

the wrapping of the region 1 currents across the noon-midnight meridian into the region 2 or 0 currents.

[66] **Acknowledgments.** This research was supported by NASA grants NAG5-10962 and NAG5-11869 and NSF grant ATM-0105032 to the University of Washington.

[67] Lou-Chuang Lee thanks the two reviewers for their assistance in evaluating this paper.

References

Birn, J., et al. (2001), Geospace Environmental Modeling (GEM) magnetic reconnection challenge, *J. Geophys. Res.*, *106*, 3715.

Biskamp, D., E. Schwartz, and J. F. Drake (1995), Ion-controlled collisionless magnetic reconnection, *Phys. Rev. Lett.*, *75*, 3850.

Chappell, C. R., T. E. Moore, and J. H. Waite Jr. (1987), The ionosphere as a fully adequate source of the Earth's magnetosphere, *J. Geophys. Res.*, *92*, 5896.

Cladis, J. B. (1986), Parallel acceleration and transport of ions from the polar ionosphere to the plasma sheet, *Geophys. Res. Lett.*, *13*, 893.

Drake, J. F., R. G. Kleva, and M. E. Mandt (1994), Structure of thin current layers: Implications for magnetic reconnection, *Phys. Rev. Lett.*, *73*, 1251.

Elphic, R. C., C. A. Cattell, K. Takahashi, S. T. Bame, and C. T. Russell (1986), ISEE-1 and 2 observations of magnetic flux ropes in the magnetotail: FTEs in the plasma sheet?, *Geophys. Res. Lett.*, *13*, 648.

Hones, J. W., Jr. (1976), The magnetotail: Its generation and dissipation, in *Physics of Solar Planetary Environments*, edited by D. J. Williams, p. 559, AGU, Washington, D.C.

Hones, J. W., Jr. (1979), Plasma flow in the magnetotail and their relation to substorms theories, in *Dynamics of the Magnetosphere*, edited by S. I. Akasofu, p. 545, D. Reidel, Norwell, Mass.

Iijima, T., and T. A. Potemra (1976), The amplitude distribution of field-aligned currents at northern high latitudes observed by Triad, *J. Geophys. Res.*, *81*, 2165.

Iijima, T., and T. A. Potemra (1978), Large-scale characteristics of field-aligned currents associated with substorms, *J. Geophys. Res.*, *83*, 599.

Lepping, R. P., D. H. Fairfield, J. Jones, L. A. Frank, W. R. Paterson, S. Kokubun, and T. Yamamoto (1995), Cross-tail magnetic flux ropes as observed by the GEOTAIL spacecraft, *Geophys. Res. Lett.*, *22*, 1193.

Lepping, R. P., J. A. Slavin, M. Hesse, J. A. Jones, and A. Szabo (1996), Analysis of magnetotail flux ropes with strong core fields: ISEE 3 observations, *J. Geomagn. Geoelectr.*, *48*, 589.

Lu, G., et al. (1996), High-latitude ionospheric electrodynamics as determined by the assimilative mapping of ionospheric electrodynamics procedure for the conjunctive SUNDIAL/ATLAS 1/GEM period of March 28–29, 1992, *J. Geophys. Res.*, *101*, 26,697.

Ma, Z. W., and A. Bhattacharjee (1996), Fast impulsive reconnection and current sheet intensification due to electron pressure gradients in semi-collisional plasmas, *Geophys. Res. Lett.*, *23*, 1673.

Moldwin, M. B., and W. J. Hughes (1991), Plasmoids as magnetic flux ropes, *J. Geophys. Res.*, *96*, 14,051.

Moldwin, M. B., and W. J. Hughes (1992), On the formation and evolution of plasmoids: A survey of ISEE 3 Geotail data, *J. Geophys. Res.*, *97*, 19,259.

Ogino, T., R. J. Walker, M. Ashour-Abdalla, and J. M. Dawson (1986), An MHD simulation pf the effects of the interplanetary magnetic field by component on the interaction of the solar wind with the Earth's magnetosphere during southward IMF, *J. Geophys. Res.*, *91*, 10,029.

Øieroset, M. T. D. Phan, M. Fujimoto, R. P. Lin, and R. P. Lepping (2001), In situ detection of collisionless reconnection in the Earth's magnetotail, *Nature*, *412*, 414.

Pritchett, P. L., F. V. Coroniti, and V. K. Decyk (1996), Three-dimensional stability of thin quasi-neutral current sheets, *J. Geophys. Res.*, *101*, 27,413.

Richtmyer, R. D., and K. W. Morton (1967), *Difference Methods for Initial Value Problems*, p. 300, Wiley-Interscience, Hoboken, N. J.

Seki, K., T. Terasawa, M. Hirahara, and T. Mukai (1998), Quantification of tailward cold O^+ beams in the lobe/mantle regions with Geotail data: Constraints on polar O^+ outflows, *J. Geophys. Res.*, *203*, 29,371.

Seki, K., R. C. Elphic, M. Hirahara, T. Terasawa, and T. Mukai (2001), On atmospheric loss of oxygen ions from Earth through magnetospheric processes, *Science*, *291*, 5510.

Shay, M. A., J. F. Drake, R. E. Denton, and D. Biskamp (1998), Structure of the dissipation region during magnetic reconnection, *J. Geophys. Res.*, *103*, 9165.

Sibeck, D. G. (1990), Evidence for flux ropes in the Earth's magnetotail, in *Physics of Magnetic Flux Ropes*, *Geophys. Mongr. Ser.*, vol. 58, edited by C. T. Russell, E. R. Priest, and L. C. Lee, p. 637, AGU, Washington, D.C.

Sibeck, D. G., G. L. Siscoe, J. A. Slavin, E. J. Smith, S. J. Bame, and F. L. Scarf (1984), Magnetotail flux ropes, *Geophys. Res. Lett.*, *11*, 1090.

Slavin, J. A., et al. (1989), CDAW-8 observations of plasmoid signatures in the geomagnetic tail: An assessment, *J. Geophys. Res.*, *94*, 15,153.

Slavin, J. A., C. J. Owen, M. Kuznetsova, and M. Hesse (1995), ISEE 3 observations of plasmoids with flux rope magnetic topologies, *Geophys. Res. Lett.*, *22*, 2061.

Sod, G. A. (1978), A survey of several finite difference methods for systems of nonlinear hyperbolic conservation laws, *J. Comput. Phys.*, *27*, 1.

Speiser, T. W. (1965), Particle trajectories in model current sheets: 1. Analytical solutions, *J. Geophys. Res.*, *70*, 4219.

Steinolfson, R. S., and R. M. Winglee (1993), Energy storage and dissipation in the magnetotail during substorms 2. MHD simulations, *J. Geophys. Res.*, *98*, 7536.

Weimer, D. R., J. R. Kanm, and S.-I. Akasofu (1992), Variations of the polar cap potential measured during magnetospheric substorms, *J. Geophys. Res.*, *97*, 3945.

Winglee, R. M. (2000), Mapping of ionospheric outflows into the magnetosphere for varying IMF conditions, *J. Atmos. Sol. Terr. Phys.*, *62*, 527.

Winglee, R. M. (2003), Circulation of ionospheric and solar wind particle populations during extended southward IMF, *J. Geophys. Res.*, *108*(A10), 1385, doi:10.1029/2002JA009819.

Winglee, R. M., and R. S. Steinolfson (1993), Energy storage and dissipation in the magnetotail during substorms: 1. Particle simulations, *J. Geophys. Res.*, *98*, 7519.

Winglee, R. M., S. Kokubun, R. P. Lin, and R. P. Lepping (1998), Flux rope structure in the magnetotail: Comparison between Wind/Geotail observations and global simulations, *J. Geophys. Res.*, *103*, 135.

Winglee, R. M., D. Chua, M. Brittnacher, G. K. Parks, and G. Lu (2002), Global impact of ionospheric outflows on the dynamics of the magnetosphere and cross-polar cap potential, *J. Geophys. Res.*, *107*(A9), 1237, doi:10.1029/2001JA000214.

Yau, A. W., and M. André (1997), Source of ion outflow in the high latitude ionosphere, *Space Sci. Rev.*, *80*, 1.

Zhu, Z., and R. M. Winglee (1996), Tearing instability, flux ropes, and the kinetic current sheet kink instability in the Earth's magnetotail: A three-dimensional perspective from particle simulations, *J. Geophys. Res.*, *101*, 4885.

R. M. Winglee, Department of Earth and Space Sciences, University of Washington, Seattle, WA 98195-1310, USA. (winglee@ess.washington.edu)